

Oxidizing octadecylphosphonic acid molecules without disrupting their self-assembled monolayers

Cite this: *Anal. Methods*, 2013, **5**, 4911

Heng-Yong Nie^{*ab}

In examination of oxidation of octadecylphosphonic acid (OPA) self-assembled monolayers (SAMs) prepared on the native oxide of a Si wafer upon exposure to UV/ozone (UVO) for up to 5 min, atomic force microscopy studies of the surface elucidated that there were no changes in morphology of the SAMs. Surprisingly, investigations on the same samples of OPA SAMs using time-of-flight secondary ion mass spectrometry revealed that the intensity of the deprotonated molecular ion fragment decreased exponentially to approximately one fourth of that of the control. We clarify that UVO-induced oxidation of alkyl chains of the OPA molecules in their SAMs precedes the disruption of the monolayer structure, which is the basis for controlling surface chemistry of SAMs with brief UVO exposure.

Received 11th April 2013

Accepted 18th July 2013

DOI: 10.1039/c3ay40612a

www.rsc.org/methods

1 Introduction

Oxidation of the surface of polymers upon their exposure to a UV/ozone (UVO) environment has been studied in detail to enhance surface wettability.^{1–3} It is believed that in the presence of UV irradiation, ozone attacks hydrocarbon chains, resulting in formation of carbon radicals, chain scission and oxidation. The oxidation of hydrocarbons leads to an increased surface energy in the treated polymer surface, enhancing their printing and adhesion applications. Due to their well-defined structures and ease of fabrication, self-assembled monolayers (SAMs)^{4,5} of organic molecules prepared on a substrate serve as a model system for the study of oxidation of hydrocarbons. For example, oxidation of thiol SAMs on Au caused by exposure to UV light in an ozone-free environment was revealed using time-of-flight secondary ion mass spectrometry (TOF-SIMS),⁶ a surface sensitive analytical technique.^{7,8} However, the most studied system is perhaps the oxidation of alkanethiol SAMs when exposed to UVO.⁹ As detected by surface enhanced Raman spectroscopy, the thiolate headgroups of dodecane thiol SAMs on Au and Ag were oxidized to sulfur oxide species in the following steps: (a) C–S bond scission and subsequent desorption of the hydrocarbon chains and (b) the exposed sulfur is oxidized to sulfite and sulfate species.¹⁰ On the other hand, it has been reported that the methyl groups of alkylsilane SAMs formed on a Si substrate can be oxidized by irradiation of vacuum UV light at 172 nm in the presence of air without the monolayer structure being altered. Being able to convert the hydrophobic methyl-terminated alkylsilane SAMs to a

hydrophilic surface has been demonstrated to be useful in building multilayers of alkylsilane SAMs.^{11,12}

Since formation of SAMs of thiols requires coinage metals as the substrate, for oxide surfaces, SAMs of organophosphonic acids have proven useful in studies of the fundamentals of SAM formation.^{13–26} Among this type of molecule, octadecylphosphonic acid (OPA) is the most studied. Experimental findings have demonstrated different speciation of OPA headgroups on different oxides. For example, OPA headgroups are bonded to an oxidized aluminum surface through the P–O–Al^{22,23} linkage formed *via* a condensation reaction between the acidic hydroxyl groups of the molecules and the hydroxyl groups on the oxide surface.^{21,22} On the other hand, it was elucidated that OPA SAMs formed on silicon oxide are anchored to the surface by hydrogen-bonding (H-bonding), making the molecules prone to attack by polar solvents and water.^{24,25} This weakly-bonded SAM system can only be achieved using a non-polar solvent having a dielectric constant of ~ 4 , which drives the polar headgroups to the medium surface. The only requirement for SAM formation using this method is physical contact between the medium and the substrate, allowing extremely fast growth of SAMs on a hydrophilic surface *via* spin-coating or dip-coating.^{24–26} This formation technique has triggered applications in organic electronics where SAMs are deposited on the dielectric to improve its compatibility with the organic semiconductor in organic thin film transistors.^{27–29}

TOF-SIMS has been used to study ion fragmentation and molecule–substrate interactions for OPA SAMs formed on mica and oxides of silicon, aluminum, hafnium and titanium.^{25,30–34} Kanta *et al.* studied the stability of OPA on a titania surface to solvent, UV and air plasma oxidation.³⁴ Water contact angle measurements and X-ray photoelectron spectroscopy (XPS) were used to assess SAM stability under those attacks. They found that the hydrophobic surface of the OPA SAMs became

^{*}Surface Science Western, The University of Western Ontario, 999 Collip Circle, London, Ontario N6G 0J3, Canada. E-mail: hnie@uwo.ca

^bDepartment of Physics and Astronomy, The University of Western Ontario, London, Ontario N6A 3K7, Canada

hydrophilic upon UVO exposure. Their XPS results showed decreased carbon content but unchanged phosphorus content, suggesting that the alkyl chains had decomposed and evaporated while the headgroups remained on the surface even after severe oxidation.

Oxidation of OPA SAMs has been studied by monitoring the increase of oxygen content with XPS and ion fragments of oxygen and phosphate groups. Its effect has been observed with decreasing water contact angle measurement.³⁴ However, there is a lack of in-depth investigations on how to relate oxidation of OPA molecules to the integrity of their SAMs and to develop TOF-SIMS analytical approaches to access the kinetics of oxidation of OPA molecules. In this article, we report a comprehensive investigation on UVO-induced oxidation of OPA SAMs prepared on a Si wafer, where the phosphonic acid headgroup is weakly attached to the native oxide surface *via* hydrogen-bonding.^{23,24} With such a well-defined molecular system having weak interactions with the substrate surface upon its exposure to UVO, we use atomic force microscopy (AFM) to evaluate morphological changes of the monolayer and TOF-SIMS to gauge oxidation of alkyl chains of the OPA molecules in the monolayer. We show that AFM is especially suitable for monitoring morphological changes of the OPA SAMs upon their exposure to UVO. Using TOF-SIMS, we study oxidation of OPA molecules by monitoring ion fragments that are characteristic to oxidation of alkyl chains. In TOF-SIMS, only an intact OPA molecule has a chance to contribute to the generation of a quasi-molecular ion fragment. Any alteration to the molecule (*e.g.*, oxidation of any part of the alkyl chains) will be reflected as a decrease in the intensity of the quasi-molecular ion fragment. We demonstrate the feasibility of using TOF-SIMS to study kinetics of oxidation of OPA SAMs induced by UVO exposure. On the basis of the experimental results obtained with the two surface analytical techniques, we elucidate that oxidation of the alkyl chains precedes morphological changes in the SAMs, which forms the grounds for controlling surface chemistry of SAMs with brief UVO exposure.

2 Experimental section

Samples of OPA SAMs were prepared with *n*-octadecylphosphonic acid [$\text{CH}_3(\text{CH}_2)_{17}\text{P}(=\text{O})(\text{OH})_2$, purity > 97%] purchased from Polycarbon Industries (Devens, MA, USA) on the native oxide layer of a Si wafer, which are denoted as OPA samples hereafter for simplicity. The Si substrates were cleaned with methanol followed by UVO exposure for 1 h using a UVO cleaner, which is described in the next paragraph. A 2 mM OPA solution in trichloroethylene was spin-coated onto the substrate. The detailed procedure of preparing OPA SAMs with full-coverage is described elsewhere.²⁴ Ten full-coverage OPA samples were prepared: five for AFM and five for TOF-SIMS analyses.

A pair of OPA samples were exposed to UVO for each specified time (3, 5, 10 and 15 min) using a UVO cleaner (Model T10×10/OES, UVOCS Inc., PA, USA) having a low pressure quartz-mercury vapor lamp emitting UV light at wavelengths of 185 nm and 254 nm. The light intensity is of the order of 10 mW

cm^{-2} .^{35,36} Hydrocarbons are excited by absorbing the 254 nm UV light, leading to their oxidation in the presence of ozone, which is generated from the oxygen in the ambient air by absorbing the 185 nm UV light. The samples were placed ~3 cm below the UV lamp. One of each pair of the UVO-treated OPA samples and the control (*i.e.*, without UVO exposure) were loaded to the TOF-SIMS instrument for analysis. The other set of samples were imaged using AFM.

Surface morphology of the OPA samples was imaged with a Park Systems XE-100 AFM in dynamic force mode, in which a cantilever with a nominal spring constant of 40 N m^{-1} and a resonance frequency of 300 kHz (MikroMasch NSC15) was vibrated at a frequency close to its resonant frequency. The apex radius of the tip that was attached to the free end of the cantilever was nominally 10 nm. The amplitude of the vibrating cantilever reduces when the tip is brought close to the sample surface (so that it is in the attractive/repulsive interactive force regime). Reduced amplitude (*e.g.*, 70% of the amplitude in free space) is used as the feedback parameter for the system to adjust the height position of the cantilever while scanning the sample surface, which constructs the surface morphology of the sample. AFM experiments were carried out in air (relative humidity ~ 50%) at room temperature.

A TOF-SIMS IV instrument from ION-TOF GmbH (Münster, Germany) was used to study oxidation of the OPA SAMs upon their exposure to UVO. A 9 keV $^{133}\text{Cs}^+$ primary ion beam produced by surface ionization from a heated cesium pellet was pulsed at a width of 600 ns before it was bunched. After bunching, the pulse width of the primary ion beam actually striking on the sample surface is reduced to <2 ns, as estimated from measuring the H^+ peak width. The primary ion beam was used to bombard the sample surface (at a fixed incident angle of 45°) to generate secondary ions. These secondary ions, either positive or negative at a time, were extracted by an electric field. They then traverse a reflectron type of flying tube and strike on the detector comprising a microchannel plate followed by a glass scintillator and a photomultiplier tube. Their arrival times were measured using a constant fraction discriminator, which are converted to mass/charge ratio (m/z) *via* calibration of known species such as hydrogen, carbon and hydrocarbons, as well as other species that are known to be present on the sample surface. In this article, H^- and C^- were used to calibrate the mass scale for negative ion mass spectra and H^+ , C^+ and Na^+ for that of positive ion mass spectra. After the extraction of the secondary ions was finished, a low energy (<20 eV) electron beam was flooded over the scanned area for charge compensation until the next pulse of the primary ion beam was shot. These events were finished within a cycle of 100 μs (or a repetition rate of 10 kHz). The base pressure of the analysis chamber of the TOF-SIMS instrument was 1×10^{-8} mbar.

The target current generated by the pulsed primary ion beam was ~2 pA, resulting in ~1200 ions per shot. The primary ion beam bombarded the sample surface with 1.2×10^6 shots over 128×128 pixels in an area of $500 \mu\text{m} \times 500 \mu\text{m}$. Hence, the primary ion dosage was $\sim 5.8 \times 10^{11} \text{ cm}^{-2}$, which is within the conventional static limit³⁷ (because this is about 0.15% of the molecular density of $4 \times 10^{14} \text{ cm}^{-2}$ of OPA SAM¹⁴). For

secondary ion mass spectra collected under these conditions, we achieved mass resolutions ($M/\Delta M$, where M is the m/z of a peak and ΔM its full width at half maximum) of 4500 and 6200 for negative ions of C_2H^- and PO_3^- , respectively, and 6200 and 8500 for positive ions of $C_2H_3^+$ and $C_3H_5^+$, respectively.

Ion mass spectra *per se* provide m/z values for numerous peaks associated with ion fragments originating mainly from the topmost monolayer of the sample surface. They will be useful when they can be assigned to elements or chemical compounds. The fidelity of assignment is expressed by the deviation of the measured m/z of a peak from the assigned ion fragment, which is defined as $\Delta = 10^6 \times (M_{\text{peak}} - M_{\text{assigned}})/M_{\text{peak}}$ in parts-per-million (ppm), and may be termed as relative mass accuracy.³⁸ With the assigned ion fragment and its Δ , the exact m/z of the peak can be calculated as $M_{\text{peak}} = M_{\text{assigned}}/(1 - \Delta \times 10^{-6})$. In this article we mention the nominal m/z of a peak (e.g., 79 for PO_3^-) rather than its exact value (of 78.9605 with $\Delta = 25$ ppm) for simplicity.

In order to compare changes in the intensities of the characteristic ion fragments as a function of UVO exposure time, Poisson-correction was applied for the dead time effect of the detecting system.³⁹ The intensities of ion fragments are normalized to the total ion intensity.

3 Results and discussion

Shown in Fig. 1 are AFM images obtained on OPA samples exposed to UVO for 0, 3, 5, 10 and 15 min. As shown in Fig. 1a–c, in comparison with the control (denoted as 0 min exposure), there are no apparent morphological changes observed in the 3 and 5 min exposed OPA samples. The root mean square roughness estimated over a scan area of $2 \mu\text{m} \times 2 \mu\text{m}$ for

images shown in Fig. 1a–c ranges from 0.07 to 0.09 nm, which is plotted in Fig. 1f. The observed invariability in surface morphology of OPA samples exposed to UVO for up to 5 min reveals that the structure of the OPA SAMs remains intact, despite oxidation of the molecules induced by UVO exposure (which will be discussed in the TOF-SIMS results to follow).

However, upon 10 min UVO exposure, the surface morphology of the OPA SAMs changes entirely (Fig. 1d): there are layer-like aggregates and droplets. The thickness of the layers is 2.5–3.0 nm, suggesting that they are not a monolayer formed by intact OPA molecules (because OPA SAMs on Si have a thickness of 2.0 nm). The tallest droplet is approximately 7.0 nm in height. In fact, we will see later from our TOF-SIMS results that there are almost no intact OPA molecules left on the surface for this OPA sample. The surface roughness for this OPA sample increases to 1.54 nm (Fig. 1f). The AFM image in Fig. 1d shows that oxidation proceeds to the extent where aggregation of (mostly) the oxidized OPA molecules eventually ruptures the monolayer structure. After UVO exposure for 15 min, as shown in Fig. 1e, there are only droplets left on the Si wafer. Those droplets have a height ranging from 4.0 to 9.0 nm and the surface roughness is now 1.36 nm.

Fig. 1d and e show that some of the substrate is exposed on the OPA samples exposed to UVO for 10 and 15 min, respectively. One can estimate from the height data that the volume of the aggregates is roughly 4.3×10^6 and $2.1 \times 10^6 \text{ nm}^3$ for the AFM images in Fig. 1d and e, respectively. With the known thickness of ~ 2.0 nm for OPA SAMs as determined by AFM and ellipsometry,⁴⁰ it is estimated that a full-coverage OPA layer over an area of $2 \mu\text{m} \times 2 \mu\text{m}$ takes a volume of $8.0 \times 10^6 \text{ nm}^3$. The AFM images shown in Fig. 1d and e suggest that the volume of the monolayer retained is approximately 54% and 26% upon

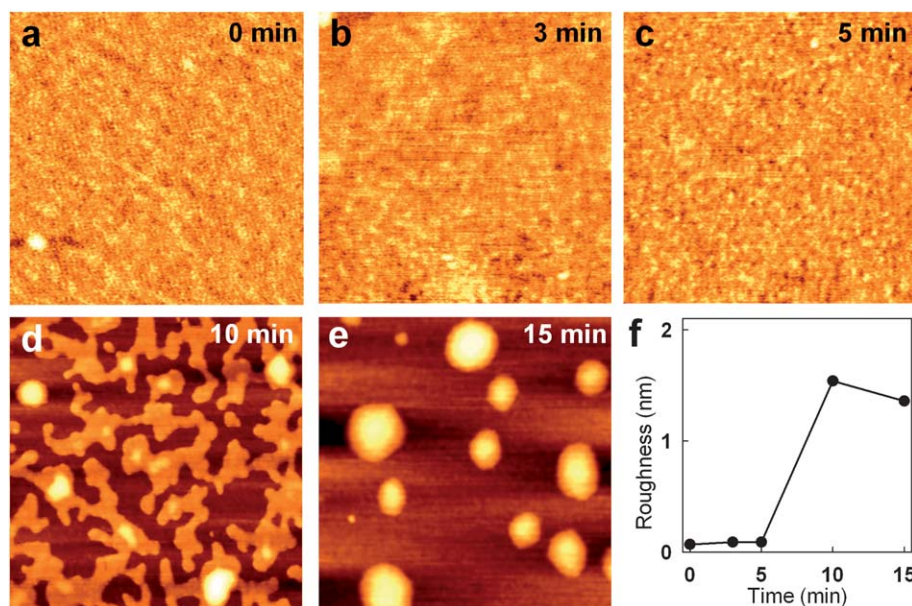


Fig. 1 AFM images (scan area: $2 \mu\text{m} \times 2 \mu\text{m}$) of OPA samples subjected to UVO exposure for (a) 0, (b) 3, (c) 5, (d) 10 and (e) 15 min, respectively. The height range for (a)–(c) is 1 nm; for (d) and (e), it is 12 and 10 nm, respectively. The area root mean square roughness estimated from images in (a)–(e) is 0.07, 0.09, 0.09, 1.54 and 1.36 nm, respectively, and plotted in (f).

UVO exposure for 10 and 15 min, respectively. This is attributable to evaporation of oxidized species (such as CO_2 and H_2O) as a result of oxidation of the hydrocarbons from the OPA alkyl chains. This observation is in agreement with that from XPS studies on UVO-treated OPA SAMs on titania, where decreases in carbon content were observed as a result of the removal of the molecules upon oxidation.³⁴

The AFM images in Fig. 1a–c show that there are no detectable morphological changes among the control, 3 and 5 min UVO-exposed OPA samples. However, we expect that the surface must be oxidized to some extent even for brief UVO exposure (e.g., 3 min). This suggests that oxidation resulting from brief UVO exposure perhaps takes place on the outmost hydrocarbons of the OPA molecules so that it does not significantly impact the structure of the monolayer. In order to investigate oxidation of the OPA SAMs as a function of UVO exposure time, we conducted TOF-SIMS experiments to analyze ion fragmentation and identify ion fragments characteristic to oxidation of OPA molecules. Before presenting the TOF-SIMS data for the oxidation investigation observed on OPA molecules weakly attached²⁵ to the oxide layer of a Si wafer *via* hydrogen-bonding (Fig. 2a), we show schematically in Fig. 2b and c the observed characteristic ion fragments of the molecule. The three major headgroup ion fragments PO_2^- , PO_3^- and PO_3H^- are shown in Fig. 2b and the two methylene-containing headgroup ion fragments of CH_3PO_3^- and $\text{C}_2\text{H}_4\text{PO}_3^-$ in Fig. 2c, respectively. The deprotonated and protonated OPA ion fragments $[\text{M} - \text{H}]^-$ and $[\text{M} + \text{H}]^+$, respectively, are depicted in Fig. 2d.

Fig. 3a shows negative (upper panel) and positive (lower panel) secondary ion mass spectra obtained on the control in the range of m/z 10 to 85. The abundant negative ion peaks OH^- , PO_2^- , PO_3^- and PO_3H^- reflect the ion fragments originating from the OPA headgroups. The two negative peaks of CH^- and C_2H^- are from the OPA alkyl chains, which are

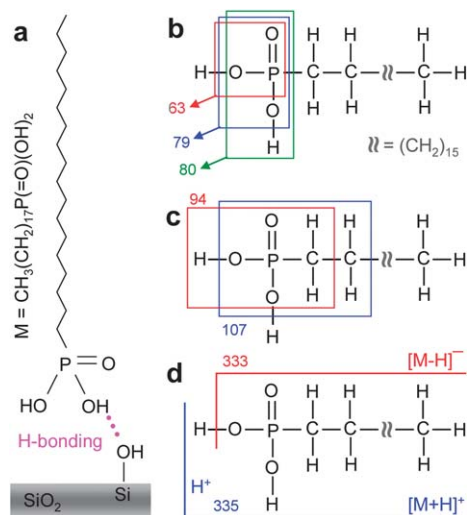


Fig. 2 The OPA molecule is attached *via* hydrogen-bonding to the silicon oxide surface (a). The fragmentation pattern of the OPA molecule is shown in (b) for the headgroup, in (c) for the headgroup with one and two methylene groups and in (d) for the quasi-molecular ion fragments.

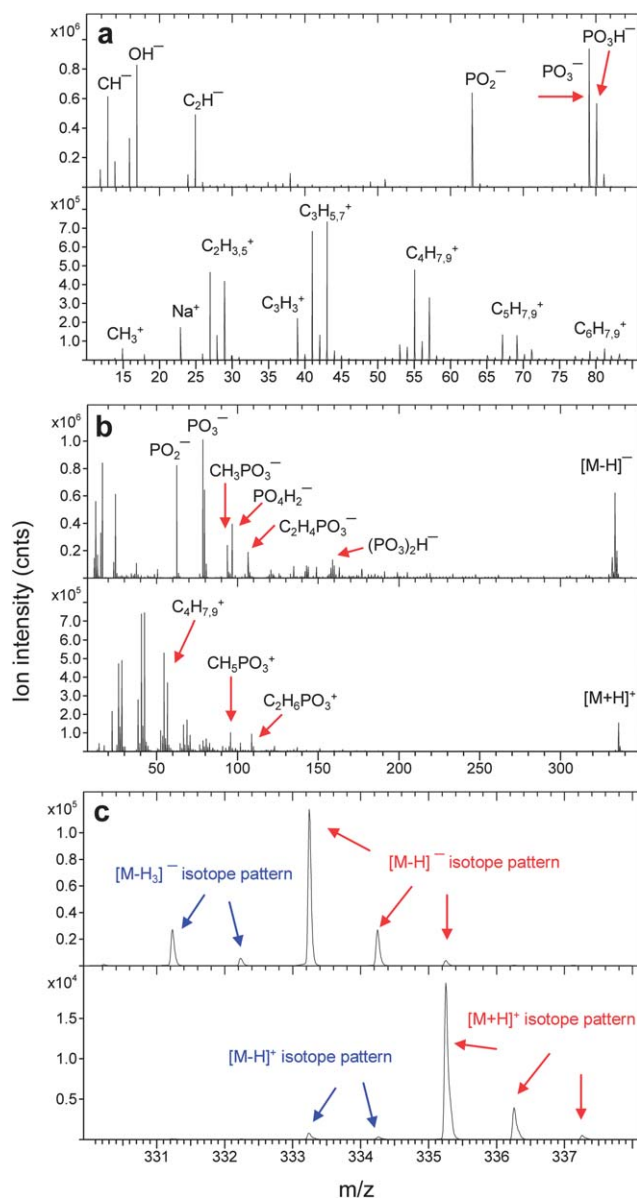


Fig. 3 Negative (upper panel) and positive (lower panel) secondary ion mass spectra obtained on the control OPA SAMs prepared on the native oxide of a Si wafer in m/z ranges of (a) 10–85, (b) 10–350 and (c) 330–338.

fragmented as positive ions of $\text{C}_n\text{H}_{2n-1}^+$ and $\text{C}_n\text{H}_{2n+1}^+$ (where $n = 2$ to 6) dominating the positive ion mass spectrum. Na^+ detected on the OPA sample is a result of surface contamination.

Shown in Fig. 3b are spectra in m/z 10–350, to compare the abundance of quasi-molecular ion fragments with the abundant ion fragments discussed in Fig. 3a. The negative ion mass spectra in Fig. 3b (upper panel) in m/z 10–350 show an abundant peak at m/z 333, which is assigned to the deprotonated molecular ion fragment $[\text{M} - \text{H}]^-$, with M representing the OPA molecular formula, $\text{CH}_3(\text{CH}_2)_{17}\text{P}(=\text{O})(\text{OH})_2$. Its abundance compares to that of the major peaks of O^- , OH^- , C_2H^- , PO_2^- and PO_3^- . As reported previously,²⁵ the abundance of $[\text{M} - \text{H}]^-$ is due to the molecule being weakly bonded to the native oxide

layer of the Si wafer. Other relatively abundant peaks identified are CH_3PO_3^- , PO_4H_2^- , $\text{C}_2\text{H}_4\text{PO}_3^-$, $(\text{PO}_3)_2\text{H}^-$, CH_5PO_3^+ and $\text{C}_2\text{H}_6\text{PO}_3^+$.

The two quasi-molecular ion fragments $[\text{M} - \text{H}]^-$ and $[\text{M} + \text{H}]^+$ are shown in Fig. 3c. The two peaks at m/z 334 and 335 of the negative ion mass spectrum are due to isotopes of carbon and hydrogen in $[\text{M} - \text{H}]^-$. The theoretical abundance of those three isotope peaks at m/z 333, 334 and 335 is 80.88%, 16.76% and 2.13%, respectively, leaving the combined abundance for the rest of the isotope peaks of $[\text{M} - \text{H}]^-$ beyond m/z 335 less than 0.3%. The abundance estimated for these three peaks from our spectrum is $83.0 \pm 0.9\%$, $15.2 \pm 0.8\%$ and $1.8\% \pm 0.1\%$, respectively, which agrees well with the theoretical ones. For the two peaks at m/z 331 and 332, because their abundance is $83.8 \pm 0.7\%$ and $14.5 \pm 0.7\%$, respectively, we infer that they are the first two isotope peaks of $[\text{M} - \text{H}_3]^-$, with the third one masked by the $[\text{M} - \text{H}]^-$ peak. For the protonated counterpart $[\text{M} + \text{H}]^+$, a similar pattern with corresponding peaks having a m/z 2 higher than those of the deprotonated counterparts is observed in the positive ion mass spectrum (lower panel of Fig. 3c).

The fragmentation of the OPA molecules is characterized by the three abundant peaks at m/z 63, 79 and 333, which are PO_2^- , PO_3^- and $[\text{M} - \text{H}]^-$. We confirmed that on a bare Si substrate, the two peaks at m/z 63 and 79 may be assigned to $^{30}\text{SiO}_2\text{H}^-$ and $^{30}\text{SiO}_3\text{H}^-$, whose intensities are rather weak. There is literally no peak at m/z 333 detected on a bare Si substrate. Therefore, these three peaks, with their high abundance, serve as the fingerprint for OPA molecules. Moreover, detection of P^- , a rather weak but distinctive peak (see Table 1 and Fig. 5b), and the protonated molecular ion fragment $[\text{M} + \text{H}]^+$ adds to ensure that a unique fragmentation pattern exists for OPA molecules.

With identification of the major peaks shown in Fig. 3, we summarize in Table 1 the identified species that are either characteristic to the OPA molecule or abundant, together with the measured m/z , their relative mass accuracy (Δ) and their intensities relative to the most abundant peak (PO_3^- and C_3H_7^+ for the negative and positive ions, respectively). The relative mass accuracy for all assigned peaks is much less than 100 ppm, which ensures that our peak assignment is reasonable. It is worth mentioning that the deprotonated OPA ion fragment $[\text{M} - \text{H}]^-$ (or $\text{C}_{18}\text{H}_{38}\text{PO}_3^-$) has a intensity close to 60% of the most abundant PO_3^- . Also listed in the table are ion fragments $\text{C}_n\text{H}_{2n}\text{PO}_3^-$ ($n = 3$ to 16) and $\text{C}_n\text{H}_{2n+2}\text{PO}_3^+$ ($n = 3$ to 7), which are much less abundant than $\text{C}_2\text{H}_4\text{PO}_3^-$ and $\text{C}_2\text{H}_6\text{PO}_3^+$, respectively, so that they are not clearly shown in Fig. 3b.

Fig. 4a and b show negative and positive ion mass spectra, respectively, for the five OPA samples in the range of m/z 8 to 340, which includes the majority of ion fragments from the OPA molecules. Also noted from the first panel of Fig. 4a and b showing the mass spectra for OPA control is that the deprotonated molecular ion fragment $[\text{M} - \text{H}]^-$ is much more abundant than its protonated counterpart $[\text{M} + \text{H}]^+$. With increasing UVO exposure time, the most noticeable change is a rapid decrease in the intensity of $[\text{M} - \text{H}]^-$ and $[\text{M} + \text{H}]^+$. Carefully inspecting ion mass spectra of both polarities leads us to the conclusion that, in terms of oxidation, negative ion mass spectra are more informative than the positive ones.

Table 1 The measured m/z , assigned ions, relative mass accuracy (Δ) and intensities (Int.) relative to the most abundant peak estimated from the secondary ion mass spectra obtained on the OPA control prepared on the native oxide layer of a Si wafer

Measured m/z	Assigned ions	Δ (ppm)	Int. (%)
Negative ions			
13.0075	CH^-	-29	43.5
15.9942	O^-	-44	19.5
17.0017	OH^-	-64	73.2
25.0075	C_2H^-	-15	43.4
30.9735	P^-	-8	0.3
46.9701	PO^-	31	0.4
62.9657	PO_2^-	34	63.2
78.9613	PO_3^-	35	100
79.9689	PO_3H^-	32	43.1
93.9863	CH_3PO_3^-	46	12.4
96.9673	PO_4H_2^-	-18	21.4
106.9942	$\text{C}_2\text{H}_4\text{PO}_3^-$	41	11.2
121.0095	$\text{C}_3\text{H}_6\text{PO}_3^-$	34	2.5
135.0274	$\text{C}_4\text{H}_8\text{PO}_3^-$	47	4.1
149.0424	$\text{C}_5\text{H}_{10}\text{PO}_3^-$	38	3.7
158.9276	$(\text{PO}_3)_2\text{H}^-$	17	5.8
163.0588	$\text{C}_6\text{H}_{12}\text{PO}_3^-$	39	3.5
177.0726	$\text{C}_7\text{H}_{14}\text{PO}_3^-$	26	2.3
191.0878	$\text{C}_8\text{H}_{16}\text{PO}_3^-$	22	2.1
205.1029	$\text{C}_9\text{H}_{18}\text{PO}_3^-$	17	1.9
219.1181	$\text{C}_{10}\text{H}_{20}\text{PO}_3^-$	14	1.7
233.1332	$\text{C}_{11}\text{H}_{22}\text{PO}_3^-$	11	1.4
247.1476	$\text{C}_{12}\text{H}_{24}\text{PO}_3^-$	5	1.1
261.1625	$\text{C}_{13}\text{H}_{26}\text{PO}_3^-$	2	1.0
275.1777	$\text{C}_{14}\text{H}_{28}\text{PO}_3^-$	0	0.8
289.1930	$\text{C}_{15}\text{H}_{30}\text{PO}_3^-$	-1	0.7
303.2072	$\text{C}_{16}\text{H}_{32}\text{PO}_3^-$	-6	0.6
333.2528	$\text{C}_{18}\text{H}_{38}\text{PO}_3^-$	-9	58.6
Positive ions			
15.0228	CH_3^+	-47	6.0
22.9911	Na^+	59	13.4
27.0224	C_2H_3^+	-41	54.0
29.0390	C_2H_5^+	-5	52.0
41.0377	C_3H_5^+	-34	86.6
43.0546	C_3H_7^+	-4	100
55.0538	C_4H_7^+	-17	55.3
57.0703	C_4H_9^+	-3	34.9
67.0533	C_5H_7^+	-22	11.5
69.0706	C_5H_9^+	3	13.7
95.9972	CH_5PO_3^+	-4	6.9
109.0053	$\text{C}_2\text{H}_6\text{PO}_3^+$	-2	6.7
123.0215	$\text{C}_3\text{H}_8\text{PO}_3^+$	3	2.4
137.0404	$\text{C}_4\text{H}_{10}\text{PO}_3^+$	26	1.7
151.0566	$\text{C}_5\text{H}_{12}\text{PO}_3^+$	28	1.3
165.0716	$\text{C}_6\text{H}_{14}\text{PO}_3^+$	22	0.8
179.0847	$\text{C}_7\text{H}_{16}\text{PO}_3^+$	6	0.3
335.2729	$\text{C}_{18}\text{H}_{40}\text{PO}_3^+$	4	8.8

It is interesting to note that there is an abundant peak at m/z 150 in the positive ion mass spectra obtained on OPA samples subjected to UVO exposure for 3 min and beyond. With observations of increased intensities of lower mass species such as NH_4^+ , CH_4N^+ and $\text{C}_2\text{H}_5\text{N}^+$ upon UVO exposure and the fact that the oxygen source is from ambient air, we speculate that this species is perhaps related to nitrogen. Its identification may be

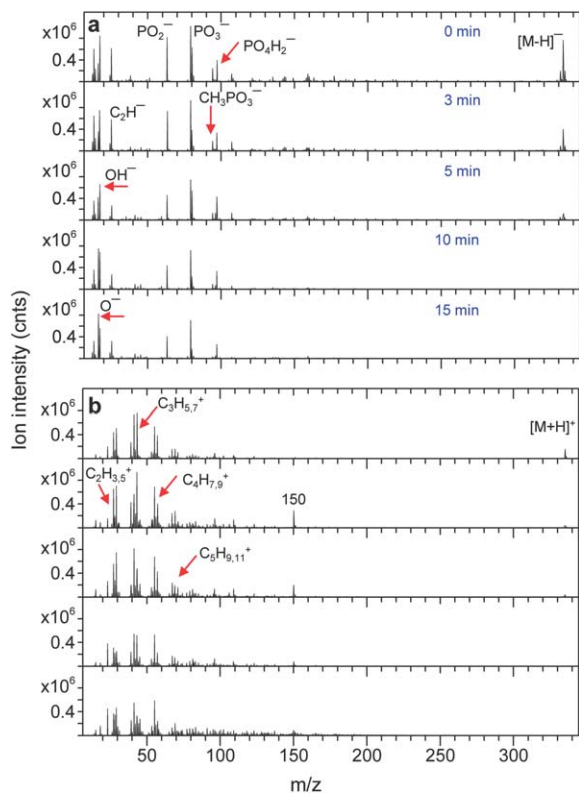


Fig. 4 Negative (a) and positive (b) ion mass spectra obtained on the five OPA samples subjected to UVO exposure for 0, 3, 5, 10 and 15 min as indicated in (a). The deprotonated and protonated OPA molecular ion fragments are denoted as $[M - H]^-$ and $[M + H]^+$, respectively, with M representing the molecular formula $\text{CH}_3(\text{CH}_2)_{17}\text{P}(=\text{O})(\text{OH})_2$.

helpful in demonstrating the usefulness of positive ion fragments in the investigation of the involvement of nitrogen in the process. Unfortunately, there is not enough information for us to identify the observed species at m/z 150. In this article, however, our aim is to examine oxidation of OPA SAMs; therefore, we concentrate on the negative ion mass spectra.

Fig. 5a–d show negative ion mass spectra in m/z ranges for C^- , CH^- , CH_2^- , O^- , OH^- , P^- , CH_3O^- , $\text{Si}_2\text{CH}_3\text{N}^-$, $\text{C}_4\text{H}_5\text{O}_2^-$, $\text{C}_5\text{H}_9\text{O}^-$, C_2HO^- , CNO^- , $\text{C}_2\text{H}_3\text{O}^-$ and $\text{C}_2\text{H}_3\text{O}^-$. Ion intensity variations for O^- , CH_3O^- , $\text{C}_4\text{H}_5\text{O}_2^-$, C_2HO^- and CHO_2^- as a function of UVO exposure time are summarized in Fig. 5e. These $\text{C}_x\text{H}_y\text{O}_z^-$ ion fragments can be assigned to structures of $\text{H}_3\text{C}-\text{O}^-$, $\text{HC}\equiv\text{C}-\text{O}^-$, $\text{H}_3\text{C}-\text{CH}=\text{CH}-\text{C}(=\text{O})-\text{O}^-$ and $\text{HC}(=\text{O})-\text{O}^-$, respectively. The increased intensities observed for those species suggest that they originate from oxidized alkyl chains of the OPA molecules. Those species are indeed characteristic species seen from polyethylene glycol and acrylic polymers.^{41,42} We have confirmed that CH_3O^- , C_2HO^- and CHO_2^- are abundant from poly(ethylene glycol) and poly(acrylic acid). CHO_2^- is also abundant from carboxylic acids and their salts. $\text{C}_4\text{H}_5\text{O}_2^-$ is the most abundant one in the negative ion fragments of $\text{C}_x\text{H}_y\text{O}_z^-$ from poly(cyclohexyl methacrylate) and other polymers of methacrylates including poly(methyl methacrylate). Assisted by the characteristic ion fragments from the polymers described above, we consider that CHO_2^- originate from carboxylates in

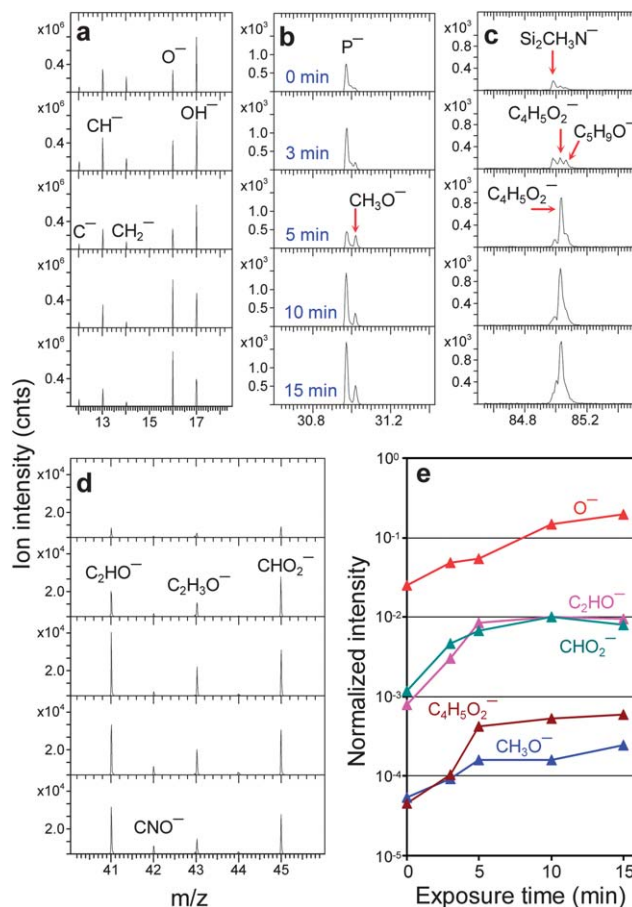


Fig. 5 Negative ion mass spectra obtained on the control (treatment time 0 min, the first panel) and four OPA samples exposed to UVO for 3, 5, 10 and 15 min as shown in the second, third, fourth and fifth panel in (b), respectively. Spectra show ion fragments of (a) O^- , (b) CH_3O^- , (c) $\text{C}_4\text{H}_5\text{O}_2^-$ and (d) C_2HO^- and CHO_2^- . The normalized ion intensity of species characteristic to oxidation as a function of UVO exposure time is shown in (e).

general and $\text{C}_4\text{H}_5\text{O}_2^-$ from methacrylic acid in particular. The detection of CH_3O^- , C_2HO^- and CHO_2^- indicates the formation of diols such as ethylene glycol. As shown above, TOF-SIMS has a unique ability to identify fragments and is thus capable of providing specific information leading to identifying oxidation of the alkyl chains. Therefore, the emergence/increase of $\text{C}_x\text{H}_y\text{O}_z^-$ serves as a marker for oxidation of the alkyl chains of OPA molecules upon their exposure to UVO.

As shown in Fig. 5e, with increasing UVO exposure time, we observed increased intensity of O^- . Since the OPA monolayer still fully covers the native SiO_2 layer of the Si substrate for samples exposed to UVO for 3 and 5 min (Fig. 1), the increase in the intensity of O^- for these two samples is inferred to be mainly derived from oxidation of the alkyl chains of OPA molecules. On the other hand, for samples exposed to UVO for 10 and 15 min, it is seen that the intensity of O^- continues to increase. From the AFM results (Fig. 1), we presume that the oxidized molecules aggregate together, which leaves exposed SiO_2 areas. Therefore, we believe that the native oxide layer of SiO_2 also contributes to the increase in the intensity of O^- observed for samples exposed to UVO for 10 and 15 min.

We thus look at ion intensities of $C_xH_yO_z^-$ species for studies on oxidation of the alkyl chains of the OPA molecules. One can see that the ion intensities of $C_xH_yO_z^-$ species increase rather rapidly on samples exposed to UVO for up to 5 min, but plateau beyond this exposure time. This is exactly the same time as the morphology of the OPA SAMs starts to change significantly (Fig. 1). This observation can be explained by considering that there is a balance between oxidation of the alkyl chains and generation of volatile species such as CO_2 and H_2O from the more severely oxidized part that is closer to the surface (*i.e.*, the tail of the alkyl chain). These two competing processes might have resulted in an almost unchanged intensity of CH_3O^- , C_2HO^- , CHO_2^- and $C_4H_5O_2^-$.

Although the increase in the ion intensities of $C_xH_yO_z^-$ species indicates oxidation of OPA molecules, they can hardly provide a quantitative analysis on how many of the molecules are affected. We thus concentrate on the variation of the ion intensity of the deprotonated OPA molecular ion fragment, $[M - H]^-$. As shown in Fig. 6a, exposure to UVO results in a rapid decrease in the intensity of $[M - H]^-$. The reason for this is because once an OPA molecule in the monolayer is changed, no matter how slightly, such an altered molecule no longer contributes to the generation of $[M - H]^-$. Therefore, its detection should serve as a sensitive marker for chemical changes (oxidation in our UVO experiment) that have occurred in the OPA molecules. Possibilities of using the intensity of $[M - H]^-$ to gauge oxidation of OPA SAMs against UVO exposure time will be investigated.

The ion intensities of $[M - H]^-$ as a function of UVO exposure time are plotted in Fig. 6b. The 3 min and 5 min UVO-exposed OPA samples have their $[M - H]^-$ intensities reduced to 47% and 27%, respectively, of that of the control, even though there are virtually no morphological changes as evidenced by the AFM images (Fig. 1b and c). The $[M - H]^-$ intensity further reduces to only about 1% of that of the control

for the 10 min UVO-exposed OPA sample. The AFM image of this OPA sample (Fig. 1d) reveals that the morphology is characterized by layer-like islands connected together and a few droplets sitting on these islands, which is a result of aggregation of the oxidized hydrocarbons. The OPA sample exposed to UVO for 15 min has less than 0.1% of $[M - H]^-$ intensity detected. At this point, there are only droplets left on the surface (Fig. 1e). Even though the matrix effect⁶ prevents us from converting the measured intensity of $[M - H]^-$ to the density of OPA molecules directly, with the largely increased intensities of $C_xH_yO_z^-$ (Fig. 5e) and the drastically reduced intensity of $[M - H]^-$ (Fig. 6b), we conclude that a good portion of the OPA molecules are oxidized upon exposure to UVO for 5 min.

As shown in Fig. 6b, the intensity of $[M - H]^-$ decreases exponentially with increasing UVO exposure time. The solid line shown in Fig. 6b represents a simulation of a first-order kinetics equation $I = I_0e^{-kt}$, where I is the intensity of $[M - H]^-$ at UVO exposure time t , I_0 the intensity at $t = 0$, with a rate constant $k = 4.5 \times 10^{-3} \text{ s}^{-1}$. The data show an excellent fit to the solid line representing the regression equation shown above, with a coefficient of determination $r^2 = 0.994$. The uncertainty of ion intensities of $[M - H]^-$ was found to be several percentages; its impact on the result presented here is negligible.

As for the estimated first-order kinetics rate constant of $4.5 \times 10^{-3} \text{ s}^{-1}$, a lack of data associated with oxidation of OPA SAMs in the literature prevents us from conducting direct comparisons. However, it has been reported that photooxidation of octanethiol and decanethiol SAMs on Ag upon UV irradiation in air follows first-order kinetics with rate constants of 1.2×10^{-2} and $1.0 \times 10^{-2} \text{ s}^{-1}$, respectively, as determined from fitting the peak intensities of the C–S stretch band with surface-enhanced Raman spectroscopy.¹⁰ Our rate constant estimated from the $[M - H]^-$ intensity decay compares with those estimated for alkanethiol SAMs with a different technique. In addition, the different UVO exposure conditions might be responsible in part for the difference seen here. While for octadecanethiol SAMs, the decay in the intensity of the C–S stretch band does not follow first-order kinetics, which is explained as the longer alkyl chains prevent their desorption necessary for C–S scission to happen,¹⁰ the decay of $[M - H]^-$ intensity observed in our experiments follows first-order kinetics, hinting that TOF-SIMS can be used to investigate kinetics of oxidation of SAMs having longer alkyl chains.

The rate of reaction is, of course, obtained under the conditions of the UVO treatment we used, which are described in the Experimental section. For other UVO systems that may have, for example, different power of UV radiation and/or ozone concentration, TOF-SIMS analyses shall reveal different rates of reaction. Therefore, it is possible to use TOF-SIMS to investigate kinetics of oxidation of SAMs with UVO exposure or other oxidation methods.

In surface chemistry modification on methyl-terminated SAMs, it is important to oxidize the SAMs to certain extent so as to keep their structural orderliness largely intact. In fact, it has been reported that UV photooxidation can be used to pattern alkanethiol SAMs formed on GaAs and Au,^{43,44} as well as alkylsilane SAMs on ITO.⁴⁵ Our analyses of OPA SAMs using

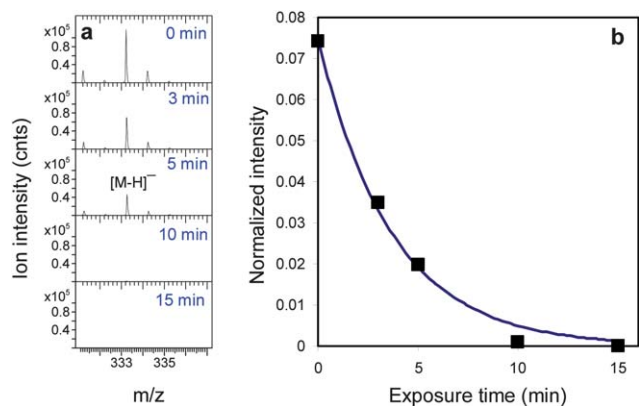


Fig. 6 Negative ion mass spectra obtained on the five OPA samples exposed to UVO for 0, 3, 5, 10 and 15 min, which are indicated in the first to fifth panels (a). Spectra show the deprotonated OPA molecular ion fragment of $[M - H]^-$, where M represents the OPA molecular formula $CH_3(CH_2)_{17}P(=O)(OH)_2$. Shown in (b) is the normalized ion intensity of $[M - H]^-$ as a function of UVO exposure time and a solid line representing simulation of a first-order kinetics equation $I = I_0e^{-kt}$, with a rate constant $k = 4.5 \times 10^{-3} \text{ s}^{-1}$.

TOF-SIMS and AFM provide an approach to figuring out the appropriate treatment time under the UVO conditions. This implies that one can readily pattern surface energy on methyl-terminated SAMs without altering the monolayer structure with the shadow mask approach: the exposed areas become hydrophilic and the masked areas remain hydrophobic.

It is worth mentioning that the molecules in OPA SAMs formed on silicon oxide are held by van der Waals forces between the alkyl chains, while the headgroups are attached to the substrate *via* H-bonding.²⁵ Such a weakly-bonded system is evidenced by the removal of OPA molecules from their SAMs upon attack by alcohols and even water.²⁴ Surprisingly, in spite of the fact that more than 70% of the OPA molecules have been oxidized upon UVO exposure for 5 min, there are no observable morphological changes in the OPA monolayer structure as evidenced from the AFM image shown in Fig. 1c. On the basis of these experimental observations, we infer that the oxidation occurred by this point (UVO exposure of 5 min) does not cause enough disruption to alter the orderliness of OPA molecules that have binding forces of van der Waals forces between alkyl chains and H-bonding between the headgroup and the substrate. When oxidation is extended to the extent that the oxidized molecules can aggregate together to form droplets, the orderliness of the monolayer structure collapses, as seen in the 10 and 15 min UVO exposed OPA samples (Fig. 1d and e).

As described above, the first-order kinetics decay of the ion intensity of $[M - H]^-$ is determined by oxidation of any portion of the OPA molecule upon UVO exposure. In order to examine oxidation of the entire alkyl chain (*i.e.*, oxidation is extended to the C-P bond), we propose to look at a negative ion fragment at m/z 94, which is assigned to CH_3PO_3^- . Fig. 7a shows the negative ion mass spectra for this species and Fig. 7c its intensity as a function of UVO exposure time. From Fig. 7a and c, it is clear that there is little change in the intensity of this species for OPA samples exposed to UVO for up to 10 min, suggesting that oxidation is not yet extended to the C-P bond. At 15 min exposure time, there is a significant decrease in the intensity of CH_3PO_3^- , indicating that a certain amount of the C-P bonds are oxidized. We confirmed that for prolonged (*e.g.*, 60 min) UVO exposure, this species almost disappeared, suggesting that the vast majority of the C-P bonds are oxidized.

By contrast, as shown in Fig. 7b and c, the intensities of the two major peaks of PO_2^- and PO_3^- remain roughly unchanged upon UVO exposure for up to 15 min. Moreover, we confirmed that even after 60 min of UVO exposure, these two species (PO_2^- and PO_3^-) were as abundant as seen here (Fig. 7b and c). Therefore, from our TOF-SIMS results, it is clear that the OPA headgroups still remain on the surface upon UVO exposure up to 15 min. Because the OPA headgroup is attached to the silicon dioxide surface initially *via* hydrogen-bonding,^{24,25} a question to ask is whether there is formation of a covalent bond after UVO exposure between the headgroup and the substrate. If the OPA headgroups become covalently bonded to the substrate, we would expect to detect ion species such as POSi^+ .

As shown in Fig. 8, we did not detect the POSi^+ ion fragment, which would be at m/z 74.9456 as indicated by the broken line. There are five well-resolved peaks within an m/z range of 0.15.

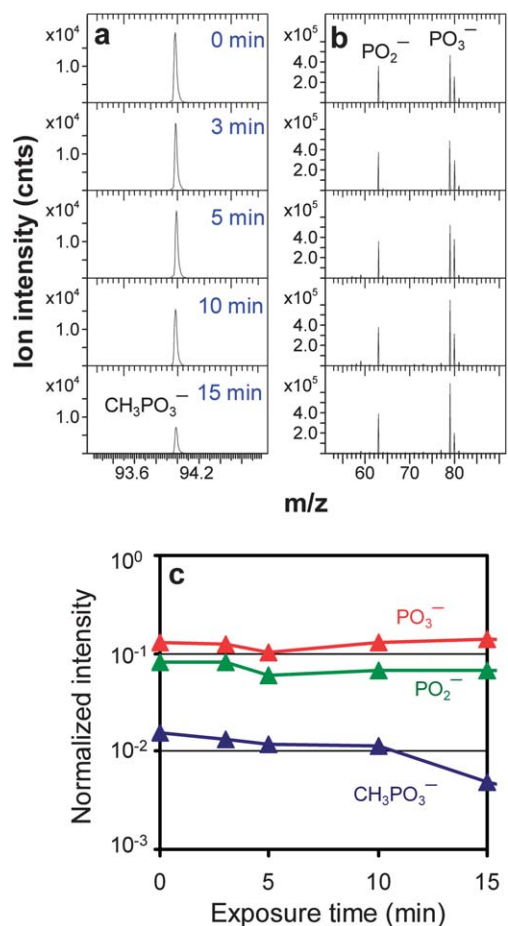


Fig. 7 Negative ion mass spectra of (a) CH_3PO_3^- and (b) PO_2^- and PO_3^- obtained on the five OPA samples exposed to UVO for 0, 3, 5, 10 and 15 min, which are indicated in the first to fifth panel of (a), respectively. Plotted in (c) is the normalized ion intensity of PO_2^- , PO_3^- and CH_3PO_3^- as a function of UVO exposure time.

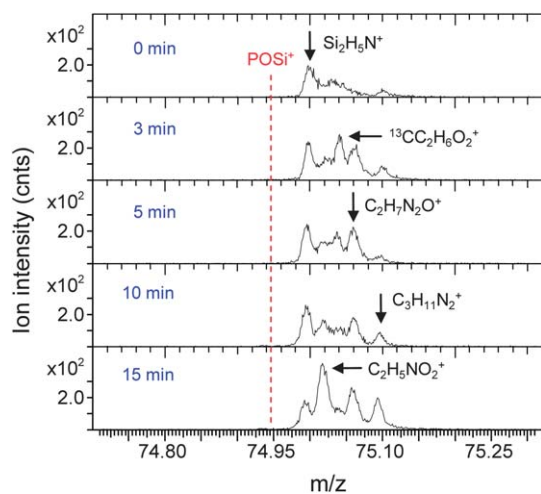


Fig. 8 Positive ion mass spectra showing lack of POSi^+ species (m/z 74.9456) for the five OPA samples exposed to UVO for 0, 3, 5, 10 and 15 min. The five peaks within the m/z range of 74.975–75.125 are used to show that the ion mass spectra have an ample mass resolution for resolving peaks that have a mere m/z difference of ~ 0.02 .

These five peaks are at m/z 74.9990, 75.0295, 75.0397, 75.0593 and 75.0923, which may be assigned to $\text{Si}_2\text{H}_5\text{N}^+$, $\text{C}_2\text{H}_5\text{NO}_2^+$, $^{13}\text{CC}_2\text{H}_6\text{O}_2^+$, $\text{C}_2\text{H}_7\text{N}_2\text{O}^+$ and $\text{C}_3\text{H}_{11}\text{N}_2^+$, respectively. Therefore, our TOF-SIMS had an ample mass resolution for a peak at m/z 74.9456 to be resolved if the POSi^+ species were to be present. From our TOF-SIMS results shown in Fig. 7 and 8, we therefore conclude that the hydrogen-bonding nature between the OPA headgroup and the substrate is not altered by UVO exposure.

4 Conclusions

Our TOF-SIMS and AFM studies of OPA SAMs formed on the native oxide layer of a Si wafer show that oxidation of the molecules upon UVO exposure precedes the disruption of the monolayer structure. We clarified that the deprotonated OPA molecular ion fragment $[\text{M} - \text{H}]^-$ is a sensitive marker for oxidation of the molecule because oxidation of any portion of it leaves no chance for the altered molecule to be fragmented as a quasi-molecular ion fragment. This is the reason behind our observation that the decay in the ion intensity of $[\text{M} - \text{H}]^-$ obeys first-order kinetics, with a rate constant of $4.5 \times 10^{-3} \text{ s}^{-1}$ determined by the conditions of the UVO system we used (a commercial UV cleaner).

Acknowledgements

The author is grateful to Surface Science Western for its continuous support of this research.

References

- 1 K. Efimenko, W. E. Wallace and J. Genzer, *J. Colloid Interface Sci.*, 2002, **254**, 306.
- 2 I. Mathieson and R. H. Bradley, *Int. J. Adhes. Adhes.*, 1996, **16**, 29.
- 3 M. J. Walzak, S. Flynn, R. Foerch, J. M. Hill, E. Karbasheski, A. Lin and M. Strobel, *J. Adhes. Sci. Technol.*, 1995, **9**, 1229.
- 4 A. Ulman, *Chem. Rev.*, 1996, **96**, 1533.
- 5 F. Schreiber, *Prog. Surf. Sci.*, 2000, **65**, 151.
- 6 A. Benninghoven, *Angew. Chem., Int. Ed. Engl.*, 1994, **33**, 1023.
- 7 N. J. Brewer, R. E. Rawsterne, S. Kothari and G. J. Leggett, *J. Am. Chem. Soc.*, 2001, **123**, 4089.
- 8 R. N. S. Sodhi, *Analyst*, 2004, **129**, 483–487; N. J. Brewer, S. Janusz, K. Critchley, S. D. Evans and J. Leggett, *J. Phys. Chem. B*, 2005, **109**, 11247.
- 9 Y. M. Zhang, R. H. Terrill and P. W. Bohn, *Chem. Mater.*, 1999, **11**, 2191.
- 10 M. Lewis, M. Tarlov and K. Carron, *J. Am. Chem. Soc.*, 1995, **117**, 9574.
- 11 Y.-J. Kim, K.-H. Lee, H. Sano, J. Han, T. Ichii, K. Murase and H. Sugimura, *Jpn. J. Appl. Phys.*, 2008, **47**, 307.
- 12 Y.-J. Kim, J. Han, H. Sano, K.-H. Lee, K. Noda, T. Ichii, K. Murase, K. Matsushige and H. Sugimura, *Appl. Surf. Sci.*, 2009, **256**, 1507.
- 13 D. K. Schwartz, *Annu. Rev. Phys. Chem.*, 2001, **52**, 107.
- 14 J. T. Woodward, A. Ulman and D. K. Schwartz, *Langmuir*, 1996, **12**, 3626.
- 15 B. R. A. Neves, M. E. Salmon, P. E. Russell and E. B. Troughton, Jr, *Langmuir*, 2000, **16**, 2409.
- 16 W. Gao, L. Dickinson, C. Grozinger, F. G. Morin and L. Reven, *Langmuir*, 1996, **12**, 6429.
- 17 I. L. Liakos, R. C. Newman, E. McAlpine and R. Alexander, *Surf. Interface Anal.*, 2004, **36**, 347.
- 18 E. L. Hanson, J. Schwartz, B. Nickel, N. Koch and M. F. Danisman, *J. Am. Chem. Soc.*, 2003, **125**, 16074.
- 19 H.-Y. Nie, M. J. Walzak and N. S. McIntyre, *Langmuir*, 2002, **18**, 2955.
- 20 H.-Y. Nie, D. J. Miller, J. T. Francis, M. J. Walzak and N. S. McIntyre, *Langmuir*, 2005, **21**, 2773.
- 21 M. J. Pellerite, T. D. Dunbar, L. D. Boardman and E. J. Wood, *J. Phys. Chem. B*, 2003, **107**, 11726.
- 22 A. Berman, S. Steinberg, S. Campbell, A. Ulman and J. Israelachvili, *Tribol. Lett.*, 1998, **4**, 43.
- 23 R. D. Ramsier, P. N. Henriksen and A. N. Gent, *Surf. Sci.*, 1988, **203**, 72.
- 24 H.-Y. Nie, M. J. Walzak and N. S. McIntyre, *J. Phys. Chem. B*, 2006, **110**, 21101.
- 25 H.-Y. Nie, *Anal. Chem.*, 2010, **82**, 3371.
- 26 H.-Y. Nie, N. S. McIntyre and W. M. Lau, *Appl. Phys. Lett.*, 2007, **90**, 203114.
- 27 Y. Ito, A. A. Virkar, S. Mannsfeld, J. H. Oh, M. Toney, J. Locklin and Z. N. Bao, *J. Am. Chem. Soc.*, 2009, **131**, 9396.
- 28 O. Acton, M. Dubey, T. Weidner, K. M. O'Malley, T.-W. Kim, G. G. Ting, D. Hutchins, J. E. Baio, T. C. Lovejoy, A. H. Gage, D. G. Castner, H. Ma and A. K.-Y. Jen, *Adv. Funct. Mater.*, 2011, **21**, 1476.
- 29 O. Acton, D. Hutchins, L. Árnadóttir, T. Weidner, N. Cernetic, G. G. Ting, T.-W. Kim, D. G. Castner, H. Ma and A. K.-Y. Jen, *Adv. Mater.*, 2011, **23**, 1899.
- 30 J. T. Francis, H.-Y. Nie, N. S. McIntyre and D. Briggs, *Langmuir*, 2006, **22**, 9244.
- 31 M. L. Jespersen, C. E. Inman, G. J. Kearns, E. W. Foster and J. E. Hutchison, *J. Am. Chem. Soc.*, 2007, **129**, 2803.
- 32 N. Adden, L. J. Gamble, D. G. Castner, A. Hoffmann, G. Gross and H. Menzel, *Langmuir*, 2006, **22**, 8197.
- 33 M. Textor, L. Ruiz, R. Hofer, A. Rossi, K. Feldman, G. Hahner and N. D. Spencer, *Langmuir*, 2000, **16**, 3257.
- 34 A. Kanta, R. Sedev and J. Ralston, *Colloids Surf., A*, 2006, **291**, 51.
- 35 M. Ouyang, P. P. Klemchuk and J. T. Koberstein, *Polym. Degrad. Stab.*, 2000, **70**, 217.
- 36 D. Q. Xiao, T. V. Le and M. J. Wirth, *Anal. Chem.*, 2004, **76**, 2055.
- 37 J. S. Fletcher, N. P. Lockyer, S. Vaidyanathan and J. C. Vickerman, *Anal. Chem.*, 2007, **79**, 2199.
- 38 F. M. Green, I. S. Gilmore and M. P. Seah, *J. Am. Soc. Mass Spectrom.*, 2006, **17**, 514.
- 39 T. Stephan, J. Zehnpfenning and A. Benninghoven, *J. Vac. Sci. Technol., A*, 1994, **12**, 405.
- 40 H.-Y. Nie, N. S. McIntyre, W. M. Lau and J. M. Feng, *Thin Solid Films*, 2008, **517**, 814.

- 41 H. K. Shon, M. Son, K. M. Park, C. K. Rhee, N. W. Song, H. M. Park, D. W. Moon and T. G. Lee, *Surf. Interface Anal.*, 2011, **43**, 628.
- 42 S. J. Hinder, C. Lowe, J. T. Maxted and J. F. Watts, *Surf. Interface Anal.*, 2004, **36**, 1575.
- 43 C. Z. Zhou and A. V. Walker, *Langmuir*, 2007, **23**, 8876.
- 44 K. S. L. Chong, S. Q. Sun and G. J. Leggett, *Langmuir*, 2005, **21**, 3903.
- 45 J. Yang, T. Ichii, K. Murase, H. Sugimura, T. Kondo and H. Masuda, *Chem. Lett.*, 2012, **41**, 392.